

1 *Conference Proceedings Paper*

## 2 **Magnetic rod-based metal-organic frameworks metal** 3 **composites for colorimetric detection of hydrogen** 4 **peroxide (H<sub>2</sub>O<sub>2</sub>) and pollutant elimination.**

5 **Benjamin Edem Meteku<sup>1\*</sup>, Jingbin Zeng<sup>2</sup> and Zifeng Yan<sup>1</sup>.**

6 <sup>1</sup> College of Chemical Engineering, China University of Petroleum (East China), Qingdao 266580, China;  
7 metekuben@yahoo.com

8 <sup>2</sup> College of Science, China University of Petroleum (East China); xmuzjb@163.com

9 \* Correspondence: metekuben@yahoo.com; (B.E.M.)

10 Received: date; Accepted: date; Published: date

11 **Abstract:** Hydrogen peroxide (H<sub>2</sub>O<sub>2</sub>) is an important oxidizing agent that plays a crucial role in the  
12 food and beverage industry, the pharmaceutical industry, environmental fields amongst others.  
13 However, as a by-product of metabolic oxidation processes, it poses an immediate danger to life and  
14 health when concentrations are beyond the minimum threshold limit of 75 ppm. The detection of  
15 H<sub>2</sub>O<sub>2</sub> is therefore of prime importance. Herein, a simple colorimetric assay for the detection of H<sub>2</sub>O<sub>2</sub>  
16 based on the peroxidase-like mimetic activity of Fe<sub>3</sub>O<sub>4</sub>@MIL-100(Fe)-Au nanozyme was established.  
17 The triad-component nanozyme was synthesized by growing a five-layer MIL-100(Fe) metal-organic  
18 framework(MOF) around the magnetic Fe<sub>3</sub>O<sub>4</sub> nanorod core and finally deposited gold on the core-  
19 shell structure. The oxidation of colorless 3,3,5,5 - tetramethylbenzidine to blue by H<sub>2</sub>O<sub>2</sub> is very slow.  
20 The addition of the nanozyme increases the oxidation process. The magnetic property of the  
21 nanozyme was further harnessed to enhance the oxidation process on a magnetic field. The versatility  
22 of the as-prepared Fe<sub>3</sub>O<sub>4</sub>@MIL-100(Fe)-Au was demonstrated by applying it for the catalytic  
23 degradation 4-nitrophenol. The magnetic property was subsequently harnessed to enhance the  
24 catalytic degradation of the organic pollutant and also to conveniently effect separation of the catalyst  
25 after application. Besides the catalysis, the magnetic property of the composite was utilized to  
26 enhance the adsorption of bacteria pathogen. We believe such magnetic MOF-based composites have  
27 potential applications in many fields including microreactor systems.

28 **Keywords:** nanozyme; metal-organic framework; peroxidase; catalysis; adsorption

### 29 **1. Introduction**

30 Nanomaterials, materials of microscopic dimensions have gained significant attention in recent  
31 years due to their outstanding properties such as optical properties, surface area, relative ease of  
32 synthesis, versatility in applications as a result of their size among others[1]. To enhance their  
33 properties and potential applications, nanomaterials are incorporated into other functional materials  
34 to obtain composite materials that were even inconceivable in the latter parts of the twentieth century.  
35 These materials are at the forefront of modern research and the synergistic effects on the properties  
36 of such materials including metal-organic frameworks, their composites and derivatives have  
37 resulted in their applications in several fields with amazing results[2]. They have successfully been

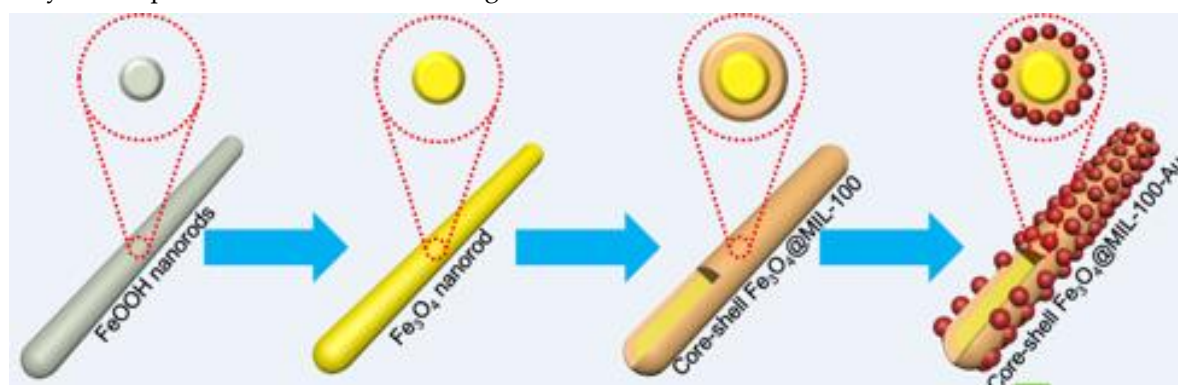
38 applied in biomedicine for cancer imaging and therapy, as antimicrobials, for energy storage, gas  
39 separation and storage, catalysis, environmental monitoring and remediation among others[3–6].  
40 Recently, nano-based materials such as MOFs have also been deployed as nanozymes, the umbrella  
41 term for an emerging paradigm that encompasses a large number of artificial nanomaterials and their  
42 composites with intrinsic enzyme-like activities[7]. They have been used for the detection of  
43 environmental pollutants, biosensing, etc.[8].

44 Hydrogen peroxide is an important chemical compound whose beneficial properties are still  
45 being explored and discoveries being made two centuries after its first successful synthesis by  
46 Thenard. Environmental concerns over deleterious chlorine-based bleaches used in the paper and  
47 allied industry resulted in the replacement of chlorine with H<sub>2</sub>O<sub>2</sub> as a bleaching agent in paper  
48 production. As a consequence, the global demand for H<sub>2</sub>O<sub>2</sub> has increased tremendously in the last  
49 decade[9]. Presently, H<sub>2</sub>O<sub>2</sub> has numerous applications from biomedicine to environmental  
50 remediation. It is applied as a mild antiseptic on the skin to prevent infections from minor cuts, and  
51 as a mouthwash in dentistry to reduce plaque and improve recovery after oral surgery[10]. During  
52 the recent outbreak of SARS CoV-2 (COVID -19), officials at Duke University and Health System  
53 successfully decontaminated N95 respirators with vaporized H<sub>2</sub>O<sub>2</sub>[11–13]. Industrially, H<sub>2</sub>O<sub>2</sub> is used  
54 as a green oxidant in processes such as in the synthesis of propene epoxide, etc in the fine chemical  
55 industry [9,14,15]. It also plays a major role in food processing and environmental remediation[16].  
56 Despite these overwhelming beneficial applications of H<sub>2</sub>O<sub>2</sub>, its presence in the human body beyond  
57 a critical threshold limit (75 ppm) is detrimental to health and can result in cell damage, inflammatory  
58 disease, cancer, etc[16–18]. The detection of H<sub>2</sub>O<sub>2</sub> is therefore of great importance due to its  
59 cytotoxicity. In this work, a magnetic MOF metal composite, Fe<sub>3</sub>O<sub>4</sub>@MIL-100(Fe)-Au was synthesized  
60 and applied as a nanozyme for the colorimetric detection of H<sub>2</sub>O<sub>2</sub>. Furthermore, the magnetic  
61 property of the nanozyme was utilized to enhance the kinetics (rate) of colorimetric detection on a  
62 magnetic field. In addition, the versatility of the synthesized composite was demonstrated by  
63 applying it for the degradation of 4-nitrophenol. Not only was the magnetic property of the  
64 composite used to enhanced the catalysis of 4-nitrophenol but also to effect separation. In addition,  
65 the property synergies of the composite were utilized for the adsorption of bacteria from solution.

## 66 2. Materials and Methods

67 The synthesis of Fe<sub>3</sub>O<sub>4</sub>@MIL-100(Fe)-Au followed three steps namely; the production of rod-  
68 shaped magnetite from rod-shaped β-FeOOH, the growth of MOF on the magnetite and the final  
69 deposition of Au on the coreshell structure. Rod-shaped β-FeOOH prepared as previously reported  
70 with slight modifications[19,20]. Briefly, 1.08 g of FeCl<sub>3</sub>.6H<sub>2</sub>O and 1.0 g of CTAB were dissolved in  
71 40 mL of deionized water. The mixture was heated at 87 °C for 12 hours under gentle stirring. After  
72 hydrolysis, the mixture was separated and the precipitate was washed with deionized water  
73 severally. The obtained precipitate (β-FeOOH) was functionalized with polyacrylic acid (PAA) and  
74 reduced in tetraethylene glycol solution at 240 °C in nitrogen (N<sub>2</sub>) environment for 8 hours. The  
75 obtained magnetic nanorods were washed severally to remove the residual chemical. Layer by layer  
76 approach was then used to build 5-layers of MOF shell around the magnetic core as previously  
77 established [21]. 20 mg equivalent of the functionalized magnetic Fe<sub>3</sub>O<sub>4</sub> nanorod was immersed in  
78 FeCl<sub>3</sub>.6H<sub>2</sub>O ethanol solution (10 mM, 4 mL) for 20 minutes at 70 °C and trimesic acid ethanol solution  
79 (10 mM, 4 mL) for 40 minutes separately at 70 °C. Between each step, the nanorods were washed with

80 ethanol and separated (process repeated for 5-cycles). Finally, reduced  $\text{HAuCl}_4$  was deposited on the  
81 magnetic core-shell structure[22] to obtain the final composite,  $\text{Fe}_3\text{O}_4@\text{MIL-100}(\text{Fe})\text{-Au}$ . A summary  
82 of the synthesis procedure is illustrated in Figure 1 below.



83

84 **Figure 1.** Schematic illustration of the synthesis of  $\text{Fe}_3\text{O}_4@\text{MIL-100}(\text{Fe})\text{-Au}$

85 The application studies was carried out by utilizing the synthesized composite for colorimetric  
86 detection of  $\text{H}_2\text{O}_2$ , degradation of 4-nitrophenol and the capture of bacteria. The peroxidase mimetic  
87 activity and the effect of the magnetic property of  $\text{Fe}_3\text{O}_4@\text{MIL-100}(\text{Fe})\text{-Au}$  were elucidated using  
88 reported protocol with slight modification[16].  $\text{Fe}_3\text{O}_4@\text{MIL-100}(\text{Fe})\text{-Au}$  (4 mg/mL, 100  $\mu\text{L}$ ) was  
89 added to sodium acetate-acetic acid buffer solution (pH =4, 2400  $\mu\text{L}$ ) followed by the addition of  
90 TMB solution (1.55mM in ethanol, 480  $\mu\text{L}$ ) and  $\text{H}_2\text{O}_2$ ( 30%, 100  $\mu\text{L}$ ). The reaction mixture was  
91 incubated for 5 minutes and subsequently followed by UV/vis analysis taking note of the absorbance  
92 at 652 nm. The colorimetric detection was carried out on a magnetic field and without magnetic field.

93 For the degradation of 4-nitrophenol, 4 mL of freshly prepared  $\text{NaBH}_4$  solution (0.2 M) was mixed  
94 with 6 mL of 4-NP solution (0.18 mM) and 4 mg of  $\text{Fe}_3\text{O}_4@\text{MIL-100}(\text{Fe})\text{-Au}$  was added to the  
95 mixture. The progress of the reaction was monitored by taking the UV-vis spectra at successive  
96 intervals. The same reduction experiment was repeated on a magnetic field for comparison purposes.  
97 At the end of each run, the composite was separated with a magnet, rinsed with deionized water,  
98 and reapplied for the next run.

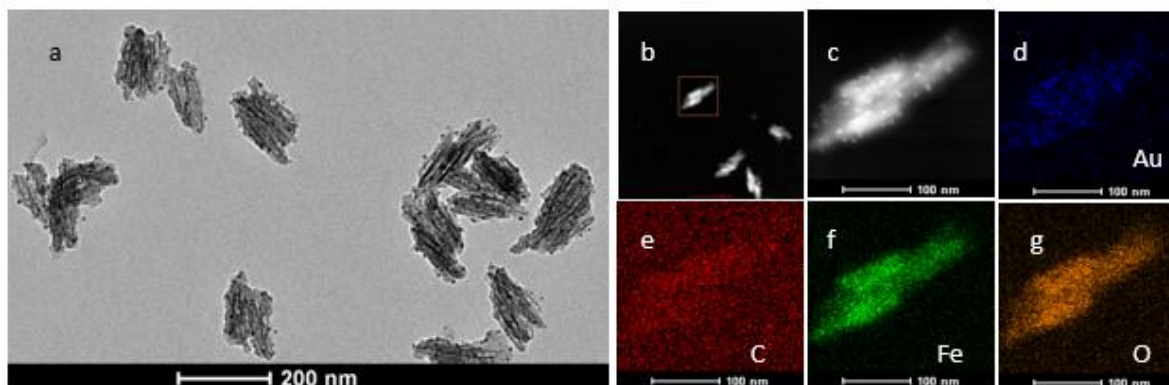
99 For the bacteria adsorption experiment, the composite was conjugated with salmonella antibody  
100 and applied for the capture of salmonella pathogen both on a magnetic field and a stationary system  
101 (non-magnetic field). The samples were stimulated at 488 nm and the corresponding fluorescence  
102 intensities were measured and capture rates determined.

### 103 3. Results and discussion

#### 104 3.1. Characterization

##### 105 3.1.1. Transmission electron microscopy (TEM) and elemental analysis

106 The TEM image in Figure 2 confirms the successful synthesis of rod-shaped magnetite  
107 structures, the successful growth of MIL-100 (Fe) shells, and the deposition of Au to form  $\text{Fe}_3\text{O}_4@\text{MIL-}$   
108  $100(\text{Fe})\text{-Au}$ . The accompanying elemental analysis also gives credence to the presence of the expected  
109 major elements in the composite (Au, C, Fe, and O)



110

111 **Figure 2.** a) TEM image of  $\text{Fe}_3\text{O}_4@\text{MIL-100(Fe)-Au}$ ; b, c) STEM HAADF image of composite;  
112 Corresponding elemental analysis results d) Au e) C f) Fe and g) O

### 113 3.1.2. X-ray diffraction (XRD) analysis

114 The X-ray diffraction analysis of the synthesized materials as exhibited in Figure 3a below shows  
115 the presence of Au with the characteristic peaks at  $2\theta = 38.2, 44.4, 64.6,$  and  $77.5^\circ$ . The characteristic  
116 peaks of magnetite and MIL-100(Fe) as observed conforms with similar observations for  $\text{Fe}_3\text{O}_4@\text{MIL-}$   
117  $100(\text{Fe})$  in literature[23].

### 118 3.1.3. Fourier transform infrared (FTIR) spectroscopy

119 The acquired FTIR as shown in Figure 3b below also confirms the formation of the synthesized  
120 composite. The characteristic stretching-vibration bands between  $3200$  and  $3600 \text{ cm}^{-1}$  which peaks at  
121  $3423 \text{ cm}^{-1}$  are indicative of OH functional groups in the preparation of  $\text{Fe}_3\text{O}_4$ . The bands at  $1550$  and  
122  $1437 \text{ cm}^{-1}$  are attributable to the C=C stretching vibrations of carboxylic acid thereby confirming the  
123 growth of MIL-100(Fe).

### 124 3.1.4. Thermogravimetric analysis (TGA)

125 Thermogravimetric analysis (TGA) was used to evaluate the thermal stability of the synthesized  
126 material and to demonstrate the successful formation of  $\text{Fe}_3\text{O}_4@\text{MIL-100(Fe)-Au}$ . As illustrated in  
127 Figure 3c, a comparison of  $\text{Fe}_3\text{O}_4@\text{MIL-100(Fe)-Au}$  and  $\text{Fe}_3\text{O}_4@\text{MIL-100(Fe)}$  reveals better stability  
128 of the composite. This can be attributed to the synergistic effect of the individual components.  
129 Besides, the significant weight loss observed in  $\text{Fe}_3\text{O}_4@\text{MIL-100(Fe)}$  is an affirmation of the successful  
130 growth of MIL-100(Fe) on the magnetite core. The successful deposition of Au results in less weight  
131 loss.

### 132 3.1.5. Vibrating-sample magnetometer (VSM) analysis

133 The magnetic property is an important feature of the prepared composite. As shown in  
134 Figure 3d, the magnetization saturation value for the composite was  $40 \text{ emu/g}$  while that of  $\text{Fe}_3\text{O}_4$   
135 nanorod was  $62 \text{ emu/g}$ . The observed difference in magnetization saturation value is due to the effect  
136 of the non-magnetic components (Au and MIL-100(Fe)) on the synthesized  $\text{Fe}_3\text{O}_4@\text{MIL-100(Fe)-Au}$ .

137

138

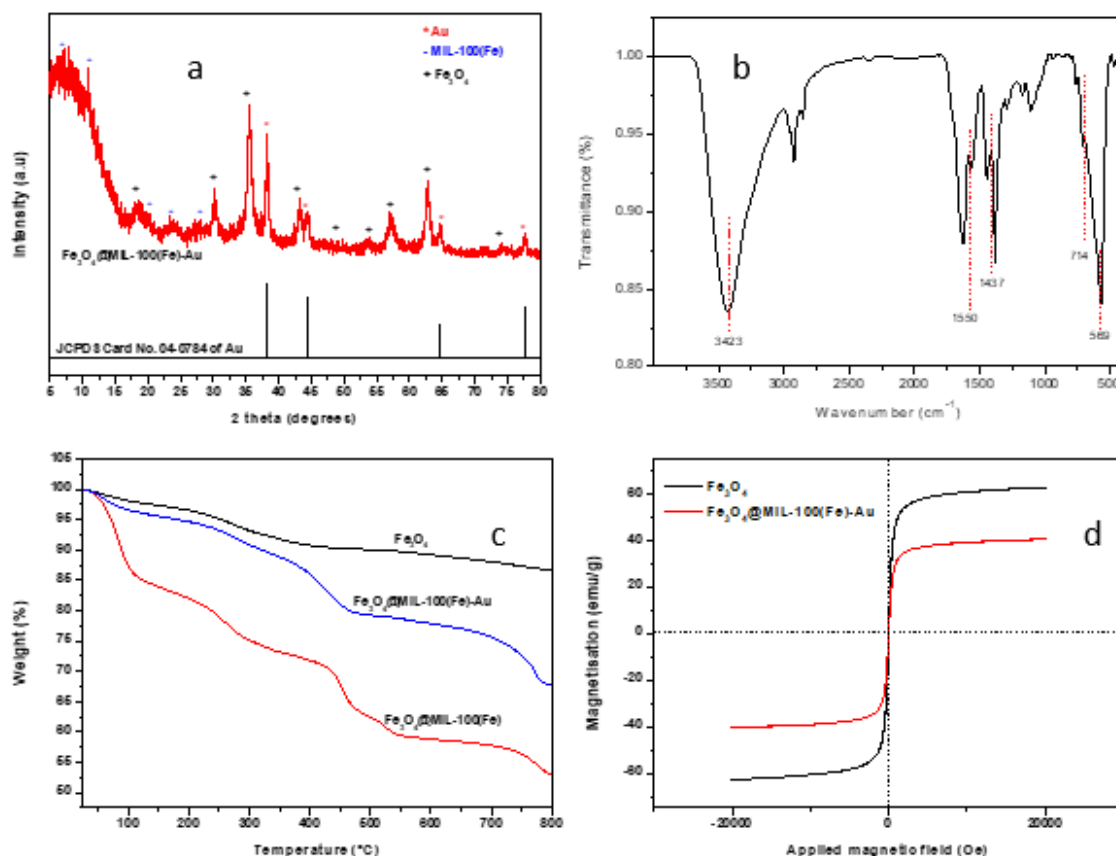
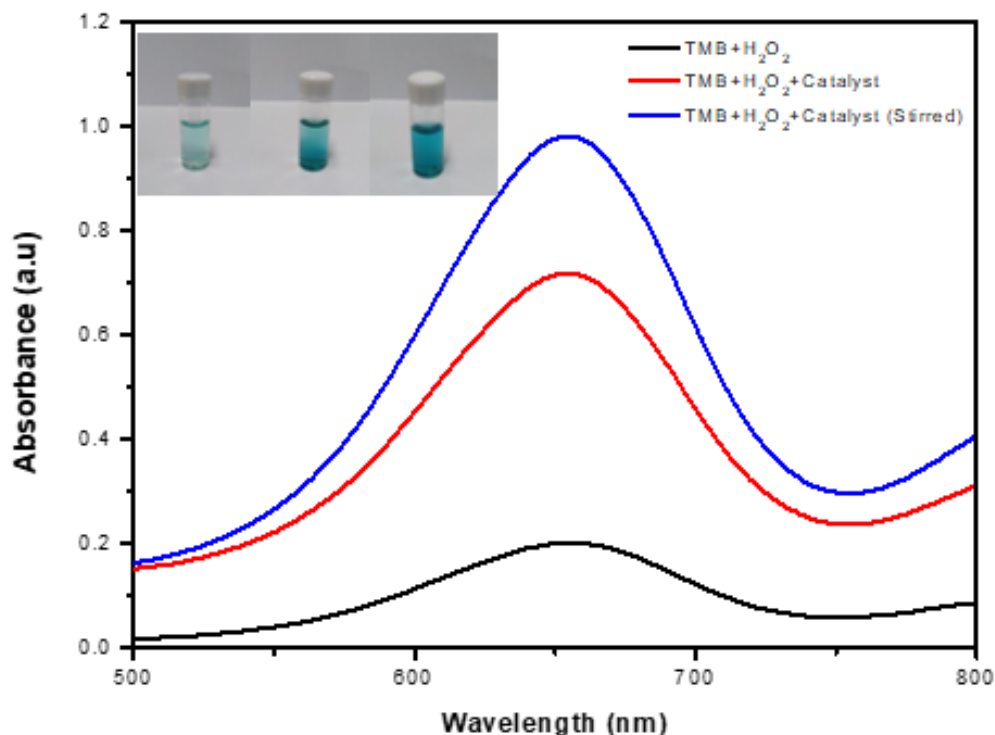


**Figure 3.** a) XRD pattern for  $\text{Fe}_3\text{O}_4$ @MIL-100(Fe)-Au; b) FTIR spectra for  $\text{Fe}_3\text{O}_4$ @MIL-100(Fe)-Au; c) Thermogram of  $\text{Fe}_3\text{O}_4$ ,  $\text{Fe}_3\text{O}_4$ @MIL-100(Fe), and  $\text{Fe}_3\text{O}_4$ @MIL-100(Fe)-Au; d) VSM plot for  $\text{Fe}_3\text{O}_4$  and  $\text{Fe}_3\text{O}_4$ @MIL-100(Fe)-Au

### 139 3.2. Application

#### 140 3.1.1. Hydrogen peroxide ( $\text{H}_2\text{O}_2$ ) detection

141 The enzyme mimetic activity of the composite was utilized for the detection of  $\text{H}_2\text{O}_2$ . The  
 142 oxidation of the colorless TMB to blue by  $\text{H}_2\text{O}_2$  after incubation for 5 minutes is very slow (no obvious  
 143 color change is observed) as shown in the picture and UV-vis spectra in Figure 4. However, upon the  
 144 addition of the nanozyme, blue color is observed after the same incubation period (Inset: middle  
 145 picture). A deep blue color was observed when the nanozyme was applied magnetic field to the reaction mixture on  
 146 a magnetic field for the same duration of incubation (Inset: left picture). The observed change in  
 147 coloration from blue to deep blue is due to the improved kinetics as a result of the stirring effect of  
 148 the nanozyme on the magnetic field. As confirmed by the associated UV-vis spectra, the magnetic  
 149 property of the nanozyme has been successfully utilized to enhance the colorimetric detection of  $\text{H}_2\text{O}_2$   
 150 (Figure 4). The observed results show that similar composites have potential applications as  
 151 nanosensors.  
 152

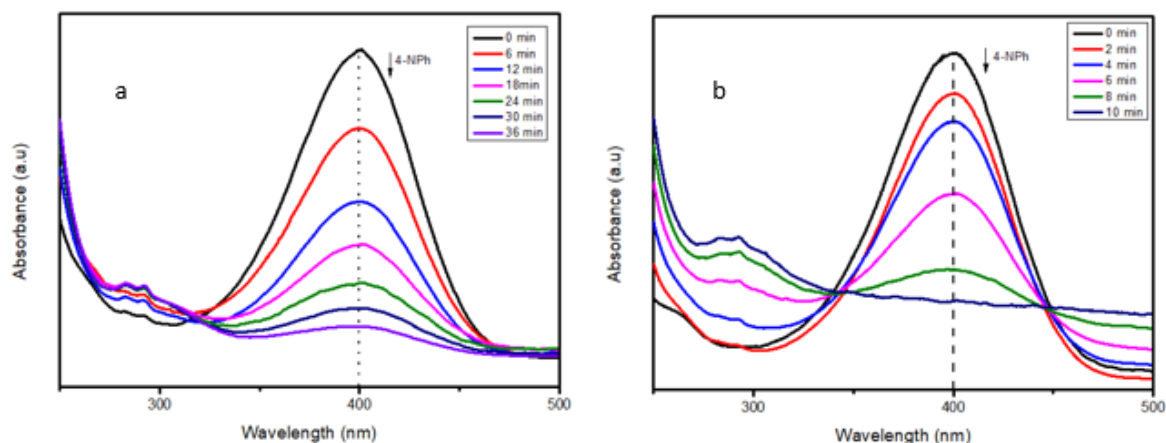


153

154 **Figure 4.** UV-vis spectra for TMB oxidation with  $H_2O_2$  without nanozyme (black), with  
 155 nanozyme (red), and with nanozyme on a magnetic field (blue) (Inset picture: TMB+ $H_2O_2$  (left), TMB  
 156 + $H_2O_2$ +Nanozyme (middle), and TMB + $H_2O_2$  + Nanozyme (on magnetic field) (right))

### 157 3.1.2. 4-nitrophenol reduction

158 The use of the synthesized composite is not limited to just colorimetric detection of  $H_2O_2$ . The  
 159 catalytic degradation of 4-nitrophenol at the presence of  $NaBH_4$  using the synthesized composite was  
 160 explored. Although  $NaBH_4$  is a strong reductant, it is unable to degrade 4-nitrophenol over a  
 161 reasonable period of time [24]. However, with the introduction of  $Fe_3O_4@MIL-100(Fe)-Au$  into the  
 162 reaction system, the degradation of 4-nitrophenol is effected as shown in Figure 5a. Furthermore, an  
 163 enhanced rate of degradation was observed when the catalysis was executed on a magnetic field as  
 164 presented in Figure 5b.

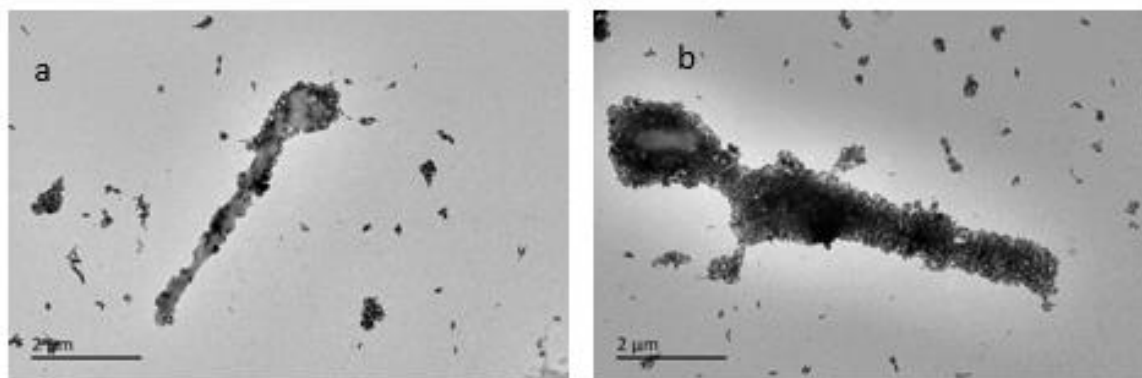


165

166 **Figure 5.** UV-vis spectra for a) Non-magnetic field-assisted catalysis of 4-nitrophenol b) Magnetic  
 167 field-assisted catalysis of 4-nitrophenol.

## 168 3.2.3. Bacteria adsorption

169 The magnetic property of exhibited by the composite was also utilized to enhance the capture of  
170 bacteria pathogen. After the composite was conjugated with antibodies of salmonella, the adsorption  
171 of salmonella pathogen was more enhanced for magnetic field-assisted adsorption as compared to  
172 the non-magnetic field-assisted adsorption (Figure 6 a and b). This observation also highlights the  
173 importance of the magnetic property of the composite.



174  
175 **Figure 6.** TEM of bacteria pathogen adsorption a) In the absence of magnetic field b) Magnetic field-  
176 assisted system.

177 **5. Conclusions**

178 In conclusion, rod-based magnetite MOF- metal composite was successfully synthesized and  
179 utilized for the colorimetric detection of the green oxidant, H<sub>2</sub>O<sub>2</sub>. The magnetic property of the  
180 composite was further harnessed to enhance the rate of detection of H<sub>2</sub>O<sub>2</sub>. Besides, the versatility of  
181 Fe<sub>3</sub>O<sub>4</sub>@MIL-100(Fe)-Au was demonstrated by successfully applying the composite for the catalytic  
182 reduction of 4-nitrophenol and for the adsorption of bacteria pathogen. In all cases, the magnetic  
183 property was utilized to enhance the kinetics of catalysis and adsorption.

184  
185 **Funding:** This research was funded by the National Natural Science Foundation of China (81501521), the  
186 Fundamental Research Funds for the Central Universities (18CX02037A), the National Key Technologies R&D  
187 Program of China, Key projects of intergovernmental international innovation cooperation (2018YFE0118200),  
188 and the Shandong Key Research and Development Project (2019JZZY010506)

189 **Conflicts of Interest:** The authors declare no conflict of interest. The funders had no role in the design of the  
190 study; in the collection, analyses, or interpretation of data; in the writing of the manuscript, or in the decision to  
191 publish the results.

192 **References**

- 193 1. Roduner, E. Size matters: why nanomaterials are different. **2006**, 583–592,  
194 doi:10.1039/b502142c.
- 195 2. Maurin, G.; Serre, C.; Cooper, A.; Férey, G. The new age of MOFs and of their porous-related  
196 solids. *Chem. Soc. Rev.* **2017**, *46*, 3104–3107, doi:10.1039/c7cs90049j.
- 197 3. Barreto, J.A.; Malley, W.O.; Kubeil, M.; Graham, B.; Stephan, H.; Spiccia, L. Nanomaterials :  
198 Applications in Cancer Imaging and Therapy. **2011**, doi:10.1002/adma.201100140.
- 199 4. Zheng, K.; Setyawati, M.I.; Leong, D.T.; Xie, J. Antimicrobial silver nanomaterials. *Coord.*  
200 *Chem. Rev.* **2018**, *357*, 1–17, doi:10.1016/j.ccr.2017.11.019.
- 201 5. Bruce, P.G.; Scrosati, B.; Tarascon, J. Lithium Batteries Nanomaterials for Rechargeable

- 202 Lithium Batteries \*\* *Angewandte*. **2008**, 2930–2946, doi:10.1002/anie.200702505.
- 203 6. Meteku, B.E.; Huang, J.; Zeng, J.; Subhan, F.; Feng, F.; Zhang, Y.; Qiu, Z.; Aslam, S.; Li, G.; Yan,  
204 Z. Magnetic metal–organic framework composites for environmental monitoring and  
205 remediation. *Coord. Chem. Rev.* **2020**, *413*, 213261, doi:10.1016/j.ccr.2020.213261.
- 206 7. Huang, P.; Yan, X.; Cai, W. Nanozyme: new horizons for responsive biomedical applications.  
207 **2019**, *48*, doi:10.1039/c8cs00718g.
- 208 8. Manuscript, A. *Environmental Science*. **2020**, doi:10.1039/C9EN01089K.
- 209 9. Ciriminna, R.; Albanese, L.; Meneguzzo, F.; Pagliaro, M. Hydrogen Peroxide : A Key Chemical  
210 for Today ' s Sustainable Development. **2016**, 1–9, doi:10.1002/cssc.201600895.
- 211 10. Vincent, M.; Thomas, U.; Christine, R. Hydrogen peroxide ( H O ): a review of its use in  
212 surgery. **2019**, 222–225, doi:10.1007/s10354-017-0610-2.
- 213 11. Beam, E.; Cih, J.C.N.; Cih, M.D.A.; Ramar, K. Effect of vaporized hydrogen peroxide  
214 reprocessing on N95 respirators. **2020**, 1–2, doi:10.1017/ice.2020.371.
- 215 12. Schwartz, A.; Stiegel, M.; Greeson, N.; Vogel, A.; Thomann, W.; Brown, M.; Sempowski, G.D.;  
216 Alderman, T.S.; Condreay, J.P.; Burch, J.; et al. Decontamination and Reuse of N95 Respirators  
217 with Hydrogen Peroxide Vapor to Address Worldwide Personal Protective Equipment  
218 Shortages During the SARS- CoV-2 ( COVID-19 ) Pandemic. **2020**, 1–4,  
219 doi:10.1177/1535676020919932.
- 220 13. Ludwig-begall, L.F.; Wielick, C.; Dams, L.; Nauwynck, H. The use of germicidal ultraviolet  
221 light , vaporized hydrogen peroxide and dry heat to decontaminate face masks and filtering  
222 respirators contaminated with a SARS-CoV-2 surrogate virus. *J. Hosp. Infect.* **2020**, 2–9,  
223 doi:10.1016/j.jhin.2020.08.025.
- 224 14. Sanderson, W.R. Cleaner industrial processes using hydrogen peroxide \*. **2000**, *72*, 1289–1304.
- 225 15. Edwards, J.K.; Solsona, B.E.; Landon, P.; Carley, A.F.; Herzing, A.; Kiely, C.J.; Hutchings, G.J.  
226 Direct synthesis of hydrogen peroxide from H 2 and O 2 using TiO 2 -supported Au – Pd  
227 catalysts. **2005**, *236*, 69–79, doi:10.1016/j.jcat.2005.09.015.
- 228 16. Sun, J.; Li, C.; Qi, Y.; Guo, S.; Liang, X. Optimizing colorimetric assay based on V2O5  
229 nanozymes for sensitive detection of H2O2 and glucose. *Sensors (Switzerland)* **2016**, *16*,  
230 doi:10.3390/s16040584.
- 231 17. Chen, A.; Chatterjee, S. Nanomaterials based electrochemical sensors for biomedical  
232 applications. *Chem. Soc. Rev.* **2013**, *42*, 5425–5438, doi:10.1039/c3cs35518g.
- 233 18. Meier, J.; Ho, E.M.; Stapleton, J.A.; Iverson, N.M. Hydrogen Peroxide Sensors for Biomedical  
234 Applications. **2019**.
- 235 19. Xu, W.; Wang, M.; Li, Z.; Wang, X.; Wang, Y.; Xing, M.; Yin, Y. Chemical Transformation of  
236 Colloidal Nanostructures with Morphological Preservation by Surface-Protection with  
237 Capping Ligands. *Nano Lett.* **2017**, *17*, 2713–2718, doi:10.1021/acs.nanolett.7b00758.
- 238 20. Wang, M.; He, L.; Xu, W.; Wang, X.; Yin, Y. Magnetic Assembly and Field-Tuning of  
239 Ellipsoidal-Nanoparticle-Based Colloidal Photonic Crystals. *Angew. Chemie - Int. Ed.* **2015**, *54*,  
240 7077–7081, doi:10.1002/anie.201501782.
- 241 21. Zhang, C.F.; Qiu, L.G.; Ke, F.; Zhu, Y.J.; Yuan, Y.P.; Xu, G.S.; Jiang, X. A novel magnetic  
242 recyclable photocatalyst based on a core-shell metal-organic framework Fe3O4@MIL-100(Fe)  
243 for the decolorization of methylene blue dye. *J. Mater. Chem. A* **2013**, *1*, 14329–14334,  
244 doi:10.1039/c3ta13030d.

- 245 22. Zhang, H.J.; Qi, S. Da; Niu, X.Y.; Hu, J.; Ren, C.L.; Chen, H.L.; Chen, X.G. Metallic  
246 nanoparticles immobilized in magnetic metal-organic frameworks: Preparation and  
247 application as highly active, magnetically isolable and reusable catalysts. *Catal. Sci. Technol.*  
248 **2014**, *4*, 3013–3024, doi:10.1039/c4cy00072b.
- 249 23. Aslam, S.; Zeng, J.; Subhan, F.; Li, M.; Lyu, F.; Li, Y.; Yan, Z. In situ one-step synthesis of  
250 Fe<sub>3</sub>O<sub>4</sub>@MIL-100(Fe) core-shells for adsorption of methylene blue from water. *J. Colloid*  
251 *Interface Sci.* **2017**, *505*, 186–195, doi:10.1016/j.jcis.2017.05.090.
- 252 24. Dong, Z.; Le, X.; Liu, Y.; Dong, C.; Ma, J. Metal organic framework derived magnetic porous  
253 carbon composite supported gold and palladium nanoparticles as highly efficient and  
254 recyclable catalysts for reduction of 4-nitrophenol and hydrodechlorination of 4-  
255 chlorophenol. *J. Mater. Chem. A* **2014**, *2*, 18775–18785, doi:10.1039/c4ta04010d.
- 256



© 2020 by the authors. Submitted for possible open access publication under the terms and conditions of the Creative Commons Attribution (CC BY) license (<http://creativecommons.org/licenses/by/4.0/>).